Journal of Mathematical Chemistry, Vol. 43, No. 4, May 2008 (© 2007)
DOI: 10.1007/s10910-007-9276-0

Equilibrium locations for nested carbon nanocones

Duangkamon Baowan* and James M. Hill

Nanomechanics Group, School of Mathematics and Applied Statistics, University of Wollongong, Wollongong, NSW 2522, Australia E-mail: db898@uow.edu.au
E-mail: jhill@uow.edu.au

Received 1 February 2007; Revised 23 February 2007

Potentially, carbon nanostructures are very important as ideal components to create many novel nano-devices. Such devices including nano-oscillators, ultra-fast optical filters and nano-bearings, are based on the unique mechanical and electronic properties of carbon nano-structures. Common carbon nanostructures used are usually C_{60}-fullerenes, carbon nanotubes, carbon nano-bundles and carbon nanotori. In the synthesis and production of carbon nanostructures, carbon nanocones tend to occur less frequently, and it is known that five different size cones may occur, depending on the number of pentagons in the atomic network. However, the simple geometric structure of carbon nanocones certainly facilitates calculations for their potential energy. Here, the Lennard–Jones potential energy function and the usual continuum approximation are employed to determine the energy for two such nested carbon nanocones which are located co-axially. We show graphically the energy profiles for any two carbon nanocones arising from the five possible structures. For both two distinct cones and two identical cones, we find that the equilibrium location moves further away from the vertex as the number of pentagons is increased. However, we observe that the equilibrium position occurs such that one cone is always inside the other, and therefore, we might expect that nested double-cones are formed according to these results.

KEY WORDS: carbon nanocones, Lennard–Jones potential, hypergeometric functions

AMS subject classification: 33C05 Classical hypergeometric functions, ${}_2F_1$, 74G65 Energy minimization

1. Introduction

Carbon nanostructures, such as C_{60}-fullerenes, carbon nanotubes and carbon nanocones, are attracting much attention as a means to create novel nano-devices. This is due to their unique properties including mechanical, electronic and their small size, high flexibility and low friction [1–3]. The most important issue in producing such devices is to understand the interatomic van der Waals potential energy behaviour between two carbon nanostructures. Much research utilizes molecular dynamics simulation to calculate the energy of carbon

* Corresponding author.

nano systems. Girifalco and his collaborators [4–6] employ the Lennard–Jones potential energy function to determine the universal graphitic systems. Zheng et al. [2, 3] use the Lennard–Jones potential energy function to determine the energy for multi-walled carbon nanotubes and propose the gigahertz frequency oscillator. This phenomena is confirmed by Legoas et al. [7]. The C_{60}-fullerenes systems are studied by Qian et al. [8, 9]. Moreover, the present authors and their colleagues employ elementary mathematical modelling to determine analytically the energy and the resulting force for such systems, (see [10–12]).

All of these investigations emphasize systems involving C_{60}-fullerenes, carbon nanotubes and carbon nanotori, but very little of the existing literature deals with carbon nanocones. Carbon nanocones have received less attention primarily because only a small amount tend to occur in the production process [13].

There are five possible ways to construct carbon nanocones depending on the number of pentagons which are needed to close the vertex, and most research on nanocones deals with their electronic structure [14, 15]. It is believed that the different number of pentagons in carbon nanocones is the key to the puzzle of nucleation in atomic construction [14, 16]. Kim et al. [17] utilize the catalytic chemical vapor deposition method to synthesize carbon nanocones inside carbon nanotubes, and they find that the resulting structures have different physical and electronic properties from the original carbon structure. Charlier and Rignanese [14] use molecular dynamics simulation to examine the local density of states for the five possible carbon nanocones and propose that carbon nanocones are ideal candidates for nanoprobes in scanning tunneling microscopy. The electronic structure of carbon nanocones is examined by Pincak and Osipov [15]. They employ the effective-mass theory for a graphite monolayer and gauge theory of disclinations on fluctuating elastic surfaces to obtain a mathematical equation, and finally they find that the electron states are dependent on the position of the pentagons. The mechanical properties of carbon nanocones are investigated by Jordan and Crespi [18]. They obtain the nonlinear mechanical behaviour for both the original shape and the inverse carbon nanocone which is obtained from the original cone by inversion.

However, from our knowledge, there is little work examining the potential energy behaviour of carbon nanocones. In this paper, we determine the potential energy for two carbon nanocones which are assumed to be co-axial. The Lennard–Jones potential energy together with the continuum approximation, which assumes that carbon atoms are uniformly distributed over the surface of each molecule, is utilized to calculate the potential energy of the system. Details for carbon nanocones are presented in the following section, and in the section thereafter we examine the geometry of cones. The interaction energy and numerical solutions for two generally distinct nested carbon nanocones are presented in sections 4 and 5, respectively, and conclusions are given in section 6. In Appendices A, and B we present mathematical details for the derivation of the

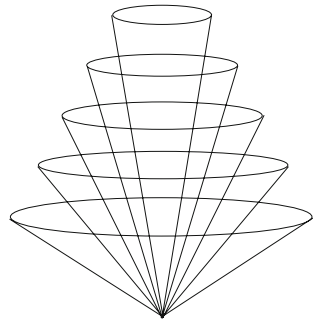

Figure 1. Five possible nanocones with vertex angles 19.20°, 38.90°, 60.00°, 83.60° and 112.90°.

potential energy for two cones which involve both hypergeometric and Legendre functions.

2. Carbon nanocones

Carbon nanocones as one of the graphitic structures were formerly discovered by Ge and Sattler [19] and subsequently synthesized by Krishnan et al. [16]. Typically, carbon nanocones are observed together with carbon nanotubes and nanotube bundles during the synthesis process [13], and carbon nanocones tend to be found at the cap of carbon nanotubes. There are five possible structures for nanocones, as shown in figure 1, because the cone angle depends on the number of pentagons needed to close the structure. Cones are formed from hexagons on a honeycombed lattice by adding fewer pentagons than the six which are needed by Euler's theorem [20] for a closed structure. In C_{60}-fullerenes, a hexagonal lattice of any size or shape can only form a closed structure by precisely twelve pentagons. The carbon nanotube cap which is a half C_{60}-fullerene contains six pentagons and therefore, carbon nanocones must have a number of pentagons which is less than six.

The disclination number of pentagons on the graphene gives the change with θ in the form

$$\theta = N_p \frac{\pi}{3},$$

where N_p is the number of the pentagons which ranges from 0 to 6. From the diagram of the cone shown in figure 2, it is clear that $\sin(\alpha/2) = r/R$ and $c = 2\pi r = 2\pi(1 - N_p/6)R$. Therefore, we obtain the relation of the cone angle and the number of pentagons as

$$\sin(\alpha/2) = 1 - \frac{N_p}{6}. \tag{1}$$

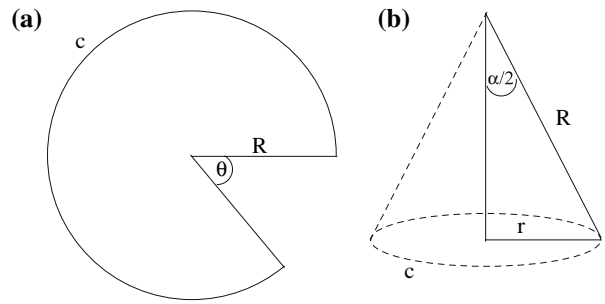

Figure 2. Graphene sheet (a) forming the carbon nanocone (b).

Table 1
Relation of number of pentagons N_p and open angle α for carbon nanocones.

Number of pentagons (N_p)	Angle of cone (α)
0	180°
1	112.90°
2	83.60°
3	60.00°
4	38.90°
5	19.2°
6	0°

There are seven possible values of the angle α depending on the number of pentagons which are shown in table 1. We note that for $N_p = 0$, we have a graphene sheet and for $N_p = 6$, we obtain a capped carbon nanotube. Hence there are only five possible values giving rise to carbon nanocones. We assume that the mean atomic surface density of carbon nanocones is the mean atomic surface density of graphene sheet which is 0.3812 Å^{-2}, due to the fact that the carbon nanocones are formed from the graphene sheet.

3. Geometry of cones

The surface shown in figure 3(a) is called a double right cone. A right cone is one for which the vertex is directly above the centre of its base. However, when used without qualification, the term cone often means right cone. A right cone is the surface in three-dimensional space generated by a line that revolves about a fixed axis in such a way that the line passes through a fixed point on the axis and always makes the same angle with the axis, and the fixed point is called the vertex of the cone. A cone consists of two parts; called nappes, that intersect at the vertex [21]. The quadratic equation in Cartesian coordinates (x, y, z) for double cones is given by

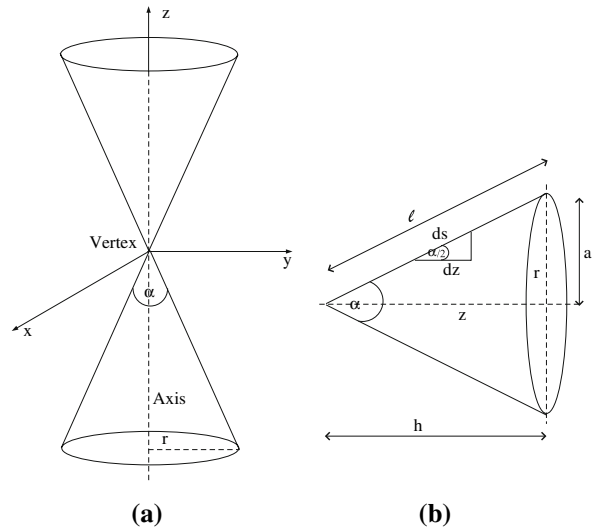

Figure 3. (a) Geometry of an elliptical cone and (b) diagram for surface integrations.

$$\frac{x^2}{a^2} + \frac{y^2}{b^2} = \frac{z^2}{c^2}, \tag{2}$$

where a, b and c are constants. Alternatively, in cylindrical coordinates (r, θ, z) the equation for the right cone can be defined as $r = z\tan(\alpha/2)$ where α is the cone angle. We need to examine the surface integral of cones to calculate the Lennard-Jones potential energy in the continuum approach. The surface area integral of a single cone is given by

$$\text{Area} = \int_0^h \int_0^{2\pi} r d\theta ds.$$

From figure 3(b), we can see that $\mathrm{d}s = \mathrm{d}z/\cos(\alpha/2)$ and $r = z\tan(\alpha/2)$. Therefore, the surface integral is of the form

$$\text{Area} = \frac{\tan(\alpha/2)}{\cos(\alpha/2)} \int_0^h \int_0^{2\pi} z\mathrm{d}\theta\mathrm{d}z = \frac{a\ell}{h^2} \int_0^h \int_0^{2\pi} z\mathrm{d}\theta\mathrm{d}z = \pi a\ell, \tag{3}$$

where $\ell = \sqrt{a^2 + h^2}$.

4. Interaction energy for carbon nanocones

4.1. *Potential energy function*

The Lennard–Jones potential, which is widely used for non-bonded atomic structures (see for example, [2, 3, 5, 6]), is adopted here to determine the

interatomic potential energy for two carbon nanocones which are located coaxially. The classical Lennard–Jones potential between a pair of atoms at a distance ρ apart is given by

$$E(\rho) = -\frac{A}{\rho^6} + \frac{B}{\rho^{12}}, \tag{4}$$

where A and B are the attractive and repulsive constants, respectively. Using the continuum approximation, which assumes that the discrete atoms may be replaced by a uniform surface density of atoms over the surface, together with the Lennard–Jones potential, the total potential energy E^{tot} for two non-bonded molecules can be obtained by performing the double surface integrals

$$E^{tot} = n_1 n_2 \int\int E(\rho) d\Sigma_1 d\Sigma_2, \tag{5}$$

where n_1 and n_2 denote mean surface densities of the first and the second molecule and ρ is the distance between surface elements $\mathrm{d}\Sigma_1$ and $\mathrm{d}\Sigma_2$.

4.2. *Model formulation for two carbon nanocones*

With reference to a rectangular Cartesian coordinate system (x_1, y_1, z_1) with origin located at the vertex of the first cone, shown in figure 4, a typical point on its surface has coordinates $(r_1 \cos\theta_1, r_1 \sin\theta_1, z_1)$. Similarly, with reference to a rectangular Cartesian coordinate system (x_2, y_2, z_2) with origin located at the vertex of the second cone, a typical point on its surface has coordinates $(r_2 \cos\theta_2, r_2 \sin\theta_2, Z + z_2)$ with respect to the coordinate system with origin located at the vertex of first cone, where Z is the distance between their vertices. The first cone has the open angle ϕ with base radius a_1 and height h_1, and $r_1 = \beta z_1$ where $\beta = \tan(\phi/2)$. The second cone has the open angle ω with base radius a_2 and height h_2, and $r_2 = \gamma z_2$ where $\gamma = \tan(\omega/2)$. The distance between two typical points on the first and the second cone is then given by

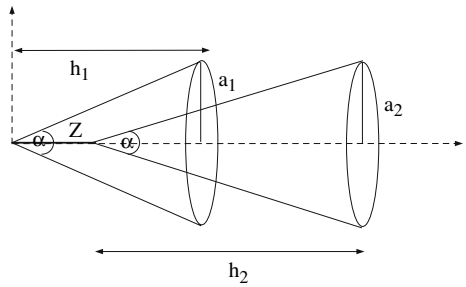

Figure 4. Geometry for two distinct carbon nanocones.

$$\begin{aligned}\rho^2 &= (r_1\cos\theta_1 - r_2\cos\theta_2)^2 + (r_1\sin\theta_1 - r_2\sin\theta_2)^2 + [z_1 - (Z+z_2)]^2,\\ &= (\beta z_1\cos\theta_1 - \gamma z_2\cos\theta_2)^2 + (\beta z_1\sin\theta_1 - \gamma z_2\sin\theta_2)^2 + [z_1 - (Z+z_2)]^2,\\ &= (\beta^2+1)z_1^2 + (\gamma^2+1)z_2^2 - 2z_1z_2(\beta\gamma+1) - 2Z(z_1-z_2) + Z^2\\ &\quad +4\beta\gamma z_1z_2\sin^2\left(\frac{\theta_1-\theta_2}{2}\right).\end{aligned}$$

By using the Lennard–Jones potential together with the continuum approximation, the total potential energy is given by

$$E^{\text{tot}} = n_1n_2\left(\frac{a_1a_2\sqrt{(a_1^2+h_1^2)(a_2^2+h_2^2)}}{h_1^2h_2^2}\right)\int_0^{h_2}\int_0^{h_1}\int_0^{2\pi}\int_0^{2\pi} z_1z_2\left(-\frac{A}{\rho^6}+\frac{B}{\rho^{12}}\right)$$
$$\times \mathrm{d}\theta_1\mathrm{d}\theta_2\mathrm{d}z_1\mathrm{d}z_2,$$

where n_1 and n_2 are mean surface densities of the first and the second carbon nanocones, respectively. Further, if we define the integrals I_n^* as

$$I_n^* = \int_0^{2\pi}\int_0^{2\pi}\frac{\mathrm{d}\theta_1\mathrm{d}\theta_2}{\rho^n} = \int_0^{2\pi}\int_0^{2\pi}\frac{\mathrm{d}\theta_1\mathrm{d}\theta_2}{\{\lambda+\xi\sin^2[(\theta_1-\theta_2)/2]\}^{n/2}}, \tag{6}$$

where $n = 6$ and 12, $\lambda = (\beta^2+1)z_1^2+(\gamma^2+1)z_2^2-2z_1z_2(\beta\gamma+1)-2Z(z_1-z_2)+Z^2$ and $\xi = 4\gamma\beta z_1z_2$. In Appendix A, we show that the integrals I_n^* can be evaluated either in terms of hypergeometric functions or Legendre functions. In terms of the hypergeometric function, we may deduce

$$I_6^* = \frac{4\pi^2}{(\lambda+\xi)^3}F\left(3,\frac{1}{2};1;\frac{\xi}{\lambda+\xi}\right),$$
$$I_{12}^* = \frac{4\pi^2}{(\lambda+\xi)^6}F\left(6,\frac{1}{2};1;\frac{\xi}{\lambda+\xi}\right).$$

These two hypergeometric functions are also degenerate hypergeometric functions, for which the details are presented in Appendix B, in the form of

$$I_6^* = \frac{4\pi^2}{\lambda^2\sqrt{\lambda(\lambda+\xi)}}\left[1-\frac{\xi}{\lambda+\xi}+\frac{3}{8}\left(\frac{\xi}{\lambda+\xi}\right)^2\right],$$
$$I_{12}^* = \frac{4\pi^2}{\lambda^5\sqrt{\lambda(\lambda+\xi)}}\left[1-\frac{5}{2}\left(\frac{\xi}{\lambda+\xi}\right)+\frac{15}{4}\left(\frac{\xi}{\lambda+\xi}\right)^2\right.$$
$$\left.-\frac{25}{8}\left(\frac{\xi}{\lambda+\xi}\right)^3+\frac{175}{128}\left(\frac{\xi}{\lambda+\xi}\right)^4-\frac{63}{256}\left(\frac{\xi}{\lambda+\xi}\right)^5\right].$$

Then the total potential energy becomes

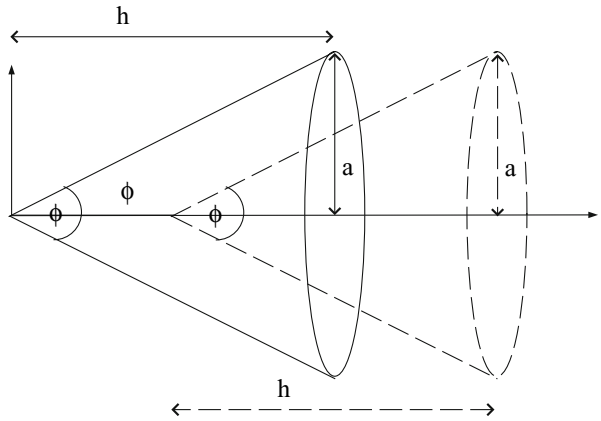

Figure 5. Geometry for two identical carbon nanocones.

$$E^{tot} = n_1 n_2 \left(\frac{a_1 a_2 \sqrt{(a_1^2 + h_1^2)(a_2^2 + h_2^2)}}{h_1^2 h_2^2} \right) \int_0^{h_2} \int_0^{h_1} z_1 z_2 (-A I_6^* + B I_{12}^*) \mathrm{d}z_1 \mathrm{d}z_2. \tag{7}$$

However, for the final solution for E^{tot}, we need to integrate (7) with respect to z_1 and z_2 which we determine numerically. Although clearly complicated numerical values for these integrals may be readily evaluated using the algebraic computer package MAPLE.

4.3. *Model formulation for identical carbon nanocones*

For the particular case, we consider the two identical carbon nanocones, as shown in figure 5, which the distance between their vertices is denoted by Z. They both have the cone angle ϕ which corresponds to base radius a and height h. The relations between r and z for both cones are given by $r_1 = \beta z_1$ and $r_2 = \beta z_2$, respectively, where $\beta = \tan(\phi/2) = a/h$. In the cylindrical polar coordinates (r, θ, z), the parametric equations for the first and the second cone can be written as $(r_1 \cos\theta_1, r_1 \sin\theta_1, z_1)$ and $(r_2 \cos\theta_2, r_2 \sin\theta_2, Z + z_2)$, respectively. Then the distance between two typical points from the first cone to the second cone is given by

$$\begin{aligned}
\rho^2 &= (r_1 \cos\theta_1 - r_2 \cos\theta_2)^2 + (r_1 \sin\theta_1 - r_2 \sin\theta_2)^2 + [z_1 - (Z + z_2)]^2, \\
&= (\beta z_1 \cos\theta_1 - \beta z_2 \cos\theta_2)^2 + (\beta z_1 \sin\theta_1 - \beta z_2 \sin\theta_2)^2 + [z_1 - (Z + z_2)]^2, \\
&= (\beta^2 + 1)(z_1 - z_2)^2 - 2Z(z_1 - z_2) + Z^2 + 4\beta^2 z_1 z_2 \sin^2[(\theta_1 - \theta_2)/2].
\end{aligned}$$

Therefore, the total potential energy can be written as

$$E^{tot} = n_\sigma^2 \left(\frac{a^4}{h^4} + \frac{a^2}{h^2}\right) \int_0^h \int_0^h \int_0^{2\pi} \int_0^{2\pi} z_1 z_2 \left(-\frac{A}{\rho^6} + \frac{B}{\rho^{12}}\right) \mathrm{d}\theta_1 \mathrm{d}\theta_2 \mathrm{d}z_1 \mathrm{d}z_2, \quad (8)$$

where n_σ is the mean surface density of the carbon nanocone. We also need to evaluate the integral

$$I_n^* = \int_0^{2\pi} \int_0^{2\pi} \frac{\mathrm{d}\theta_1 \mathrm{d}\theta_2}{\rho^n} = \int_0^{2\pi} \int_0^{2\pi} \frac{\mathrm{d}\theta_1 \mathrm{d}\theta_2}{\{\lambda + \xi \sin^2[(\theta_1 - \theta_2)/2]\}^{n/2}}, n = 6, 12,$$

where in this case $\lambda = (\beta^2 + 1)(z_1 - z_2)^2 - 2Z(z_1 - z_2) + Z^2$ and $\xi = 4\beta^2 z_1 z_2$. By precisely the same method, we may deduce

$$E^{tot} = n_\sigma^2 \left(\frac{a^4}{h^4} + \frac{a^2}{h^2}\right) \int_0^h \int_0^h z_1 z_2 (-A I_6^* + B I_{12}^*) \mathrm{d}z_1 \mathrm{d}z_2, \quad (9)$$

which we have also evaluated numerically to obtain the final solution for E^{tot}.

5. Numerical solutions

In this section, we show graphically the potential energy for two carbon nanocones of the five possible structures. Using the algebraic package MAPLE, we plot the relation between the potential energy and the distance between their vertices Z. Due to the lack of the Lennard–Jones constants, namely the attractive constant A and repulsive constant B, specifically for carbon nanocones, we then employ the Lennard–Jones constants for carbon-carbon atoms for the carbon nanocones. Following the work of Girifalco [4], we obtain $A = 19.97\,\mathrm{eV\AA}^6$ and $B = 34.81 \times 10^3\,\mathrm{eV\AA}^{12}$. The values of a and h are given by $a = \sin(\alpha/2)\ell = 3m\bar{a}\sin(\alpha/2)/2$ and $h = \cos(\alpha/2)\ell = 3m\bar{a}\cos(\alpha/2)/2$, where m is a positive integer which is indicated the size of carbon nanocones. Here, we choose $m = 50$.

We examine the potential energy for the system of the two carbon nanocones which are explicitly shown in figures 6–8. For the combination of the cone containing one pentagon, the equilibrium location for the other four cones occurs at approximately at 3 Å for the distance between their vertices, illustrated in figure 6, and the most stable equilibrium location happens for the cone $N_p = 2$. The equilibrium location increases and the system has less stability as the number of pentagons increases, and this is shown in figure 7. Of particular interest for two identical carbon nanocones, the increased number of carbon atoms at the vertex causes the distance between their vertices at the equilibrium position to increase as demonstrated in figure 8. Values of the distances between their vertices Z at the equilibrium location for any two carbon nanocones are given in table 2.

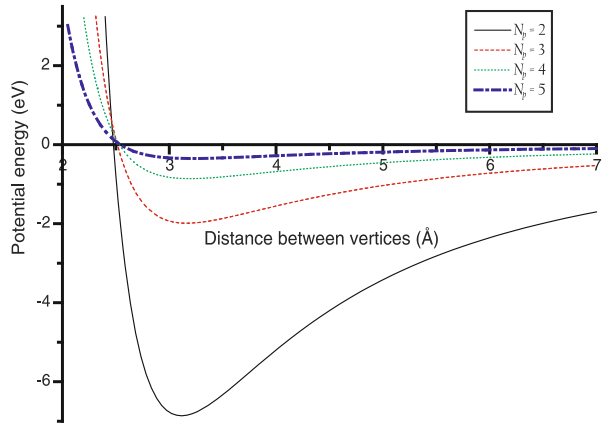

Figure 6. Variation of potential energy versus the distance between vertices for the cone $N_p = 1$ and $N_p = 2, 3, 4$ and 5 for the second cone.

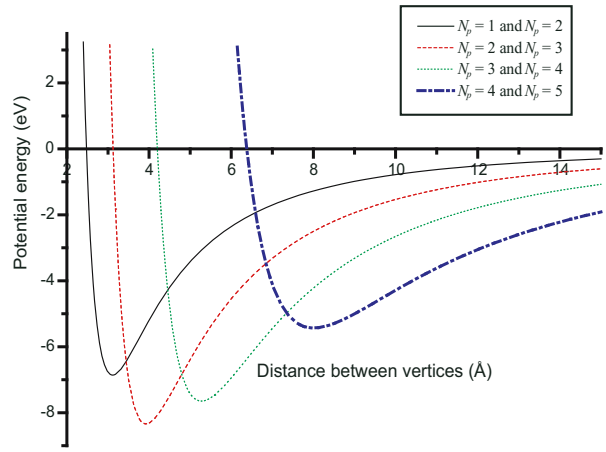

Figure 7. Variation of potential energy versus the distance between vertices for various combinations of two different cones.

The shortest distance between the two cones at the equilibrium location is denoted by x as illustrated in figure 9 and values of x are shown in table 3. For the two identical carbon nanocones, we obtain the value of 3.4 Å, which is the inter-spacing distance for two graphene sheets. Otherwise, we get values of approximately 2.6 Å which is less than the equilibrium location for two graphene sheets due to the fact that the two surfaces are not parallel. We observe that x increases with increasing number of pentagons.

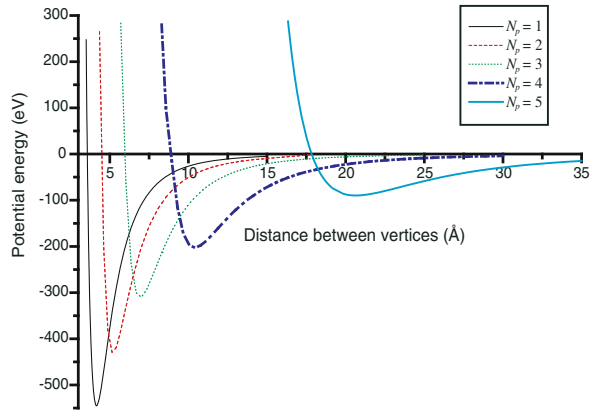

Figure 8. Variation of potential energy versus the distance between vertices for five identical carbon nanocones.

Table 2
Distance between vertices Z at the equilibrium position for any two carbon nanocones.

N_p of inner cone N_p of outer cone	1	2	3	4	5
1	4.1631	3.1161	3.1614	3.2001	3.2110
2	–	5.2663	3.9256	3.9973	4.0197
3	–	–	6.9211	5.2785	5.3703
4	–	–	–	10.3732	8.0004
5	–	–	–	–	20.6060

6. Conclusions

In this paper we determine the potential energy for two carbon nanocones for both cases of identical and non-identical cones. Using the Lennard–Jones potential energy and the continuum approximation, which assumes that the discrete carbon atoms can be replaced by an average distribution over each surface, we perform the integration of the Lennard–Jones potential energy. Due to the lack of specific data for carbon nanocones, we employ for the carbon nanocones the known Lennard–Jones constants determined for plane sheets of carbon–carbon atoms. We obtain a value 3 Å for the distance between the two vertices at the equilibrium position for the system of two identical one pentagon cones, and if this cone is paired with the other four possible cones, then this distance increases with decreasing cone angle or increasing number of pentagons. Moreover, in the case of two identical carbon nanocones, the equilibrium position moves away from the vertex as we reduce the cone angle. However, the equilibrium location is always inside the cone, and therefore as a result, we might construct

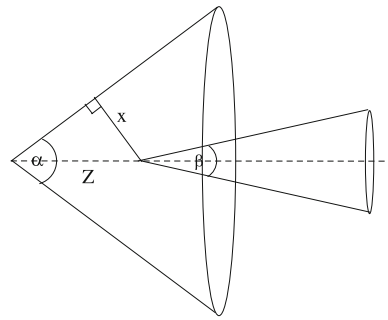

Figure 9. Shortest distance x between two carbon nanocones at the equilibrium location.

Table 3
Shortest distance x between the two cones at the equilibrium position for any two carbon nanocones.

N_p of inner cone N_p of outer cone	1	2	3	4	5
1	3.4695	2.5970	2.6347	2.6670	2.6761
2	–	3.5101	2.6165	2.6643	2.6793
3	–	–	3.4606	2.6393	2.6852
4	–	–	–	3.4541	2.6640
5	–	–	–	–	3.4364

nested double-cones from any two possible combinations of carbon nanocones as shown in figure 9.

Acknowledgements

The authors are grateful to the Australian Research Council for support through the Discovery Project Scheme and JMH is grateful for the award of an Australian Professorial Fellowship. They are also especially grateful to their colleagues Barry Cox, Ngamta Thamwattana and Tamsyn Hilder for many helpful comments and discussions on this work.

Appendix

A Analytical solution for I_n^* in (6)

The integral (6) may be evaluated either in terms of hypergeometric of Legendre functions. First we consider the integral

$$I_{2m}^{*} = \int_0^{2\pi}\int_0^{2\pi} \frac{\mathrm{d}\theta_1 \mathrm{d}\theta_2}{\{\lambda + \xi \sin^2[(\theta_1 - \theta_2)/2]\}^m}, \tag{10}$$

where $m = n/2$. However, since the integrand is a symmetric function θ_1–θ_2, the intermediate integral I_{2m}^{**} defined by

$$I_{2m}^{**} = \int_0^{2\pi} \frac{\mathrm{d}\theta_1}{\{\lambda + \xi \sin^2[(\theta_1 - \theta_2)/2]\}^m},$$

can be shown by differentiation with respect to θ_2 to be independent of θ_2, namely

$$\frac{\mathrm{d}I_{2m}^{**}}{\mathrm{d}\theta_2} = \int_0^{2\pi} -\frac{\partial}{\partial\theta_1}\left(\frac{1}{\{\lambda + \xi \sin^2[(\theta_1 - \theta_2)/2]\}^m}\right)\mathrm{d}\theta_1 = 0.$$

Thus, we may set θ_2 to be zero and trivially perform the θ_2 integration so that (10) becomes,

$$I_{2m}^{*} = 8\pi \int_0^{\pi/2} \frac{\mathrm{d}x}{(\lambda + \xi \sin^2 x)^m},$$

and we may consider the integral I_{2m} defined by

$$I_{2m} = \int_0^{\pi/2} \frac{\mathrm{d}x}{(\lambda + \xi \sin^2 x)^m}. \tag{11}$$

Making the substitution $t = \cot x$ we obtain

$$I_{2m} = \int_0^{\infty} \frac{(1+t^2)^{m-1}}{(\lambda + \xi + \lambda t^2)^m}\mathrm{d}t = \frac{1}{(\lambda+\xi)^m}\int_0^{\infty} \frac{(1+t^2)^{m-1}}{(1+\gamma t^2)^m}\mathrm{d}t,$$

where $\gamma = \lambda/(\lambda + \xi)$. Now on writing this integral in the form

$$I_{2m} = \frac{1}{(\lambda+\xi)^m}\int_0^{\infty} \frac{1}{[1-(1-\gamma)t^2/(1+t^2)]^m}\frac{\mathrm{d}t}{(1+t^2)},$$

we are led to make the substitution

$$z = \frac{t}{(1+t^2)^{1/2}}, \qquad t = \frac{z}{(1-z^2)^{1/2}}, \qquad \mathrm{d}t = \frac{\mathrm{d}z}{(1-z^2)^{3/2}},$$

and in the following line we make the substitution $u = z^2$

$$\begin{aligned} I_{2m} &= \frac{1}{(\lambda+\xi)^m}\int_0^1 \frac{\mathrm{d}z}{[1-(1-\gamma)z^2]^m(1-z^2)^{1/2}} \\ &= \frac{1}{2(\lambda+\xi)^m}\int_0^1 \frac{u^{-1/2}(1-u)^{-1/2}}{[1-(1-\gamma)u]^m}\mathrm{d}u. \end{aligned}$$

From Gradshteyn and Ryzhik [24] (p. 995, equation 9.111) we may deduce

$$I_{2m} = \frac{\pi}{2(\lambda+\xi)^m} F\left(m, \frac{1}{2}; 1; \frac{\xi}{\lambda+\xi}\right), \tag{12}$$

where $F(a, b; c; z)$ denotes the usual hypergeometric function. We comment that Colavecchia et al. [22] examine in some detail the numerical evaluation of various hypergeometric functions.

From Erdélyi [23] and on recognizing two of the numbers $\pm(1-c)$, $\pm(a-b)$, $\pm(a+b-c)$ are equal to each other, it can be shown that this result admits a quadratic transformation and becomes a Legendre function. Using the transformation

$$F(a, b; 2b; 4z/(1+z)^2) = (1+z)^{2a} F(a, a+1/2-b; b+1/2; z^2),$$

we obtain

$$I_{2m} = \frac{\pi(1+y)^{2m}}{2(\lambda+\xi)^m} F(m, m; 1; y^2),$$

where $4y/(1+y)^2 = \xi/(\lambda+\xi)$. Using the definitions from Gradshteyn and Ryzhik [24] (p. 960, equation 8.772.3 and p. 998, equation 9.131.1)

$$P_\nu^\mu(z) = \frac{1}{\Gamma(1-\mu)} \left(\frac{z-1}{z+1}\right)^{-\mu/2} \left(\frac{z+1}{2}\right)^\nu F\left(-\nu, -\nu-\mu; 1-\mu; \frac{z-1}{z+1}\right),$$

and

$$F(a, b; c, z) = (1-z)^{c-a-b} F(c-a, c-b; c; z),$$

where $P_\nu^\mu(z)$ is a Legendre function of the first kind and in our case μ is zero, then we obtain the integral in terms of the Legendre function which is given by

$$I_{2m} = \frac{\pi}{2(\lambda+\xi)^m} \left(\frac{1+y}{1-y}\right)^m P_{m-1}\left(\frac{1+y^2}{1-y^2}\right). \tag{13}$$

B Degenerate hypergeometric functions

The details of the degenerate hypergeometric function of (12) are presented in this appendix. The degenerate hypergeometric function is the hypergeometric function which can be written as the finite summation of the polynomial. For convenience, we define 4

$$J_m = F(m, 1/2; 1; z), \tag{14}$$

where m is a positive integer. Following Erdélyi [23], equation (14) admits the degenerate hypergeometric function in the case number 16 (p.72) with a agenerated solution

$$F(a,b;c;z) = (1-z)^{c-a-b}F(c-a,c-b;c;z).$$

Then we obtain

$$J_m = (1-z)^{1/2-m}F(1-m,1/2;1;z). \tag{15}$$

In terms of a series, the hypergeometric function is given by

$$F(a,b;c;z) = \sum_{n=0}^{\infty} \frac{(a)_n(b)_n}{n!(c)_n} z^n,$$

where

$$(a)_n = \Gamma(a+n)/\Gamma(a) = a(a+1)(a+2)\ldots(a+n-1) \quad \text{and} \quad (a)_0 = 1.$$

Here, we need to evaluate J_3 and J_6, and from (15) we may deduce

$$\begin{aligned} J_3 &= \frac{1}{(1-z)^{5/2}} \sum_{n=0}^{2} \frac{(-2)_n(1/2)_n}{n!(1)_n} z^n = \frac{1}{(1-z)^{5/2}} \left(1 - z + \frac{3}{8}z^2\right), \\ J_6 &= \frac{1}{(1-z)^{11/2}} \sum_{n=0}^{5} \frac{(-5)_n(1/2)_n}{n!(1)_n} z^n \\ &= \frac{1}{(1-z)^{11/2}} \left(1 - \frac{5}{2}z + \frac{15}{4}z^2 - \frac{25}{8}z^3 + \frac{175}{128}z^4 - \frac{63}{256}z^5\right). \end{aligned} \tag{16}$$

References

[1] J. Cumings and A. Zettl, Science 289 (2000) 602.
[2] Q. Zheng and Q. Jiang, Phys. Rev. Lett. 88 (2002) 045503.
[3] Q. Zheng, J.Z. Liu, and Q. Jiang, Phys. Rev. B 65 (2002) 245409.
[4] L.A. Girifalco J. Phys. Chem. 96 (1992) 858.
[5] L.A. Girifalco, M. Hodak, and R.S. Lee, Phys. Rev. B 62 (2000) 13104.
[6] M. Hodak and L.A. Girifalco, Chem. Phys. Lett. 250 (2001) 405.
[7] S.B. Legoas, V.R. Coluci, S.F. Braga, P.Z. Coura, S.O. Dantas and D.S. Galvão, Phys. Rev. Lett. 90 (2003) 055504.
[8] D. Qian, W.K. Liu and R.S. Ruoff, J. Phys. Chem. B 105 (2001) 10753.
[9] D. Qian, W.K. Liu, S. Subramoney, R.S. Ruoff, J. Nanosci. Nanotech. 3 (2003) 185.
[10] D. Baowan and J.M. Hill, Z. Angew. Math. Phys. 58 (2007).
[11] B.J. Cox, N. Thamwattana and J.M. Hill, Proc. R Soc. A 463 (2007) 461.
[12] B.J. Cox, N. Thamwattana and J.M. Hill, Proc. R Soc. A 463 (2007) 477.
[13] K. Sattler, Carbon 33 (1995) 915.
[14] J.C. Charlier and G.M. Rignanese, Phys. Rev. Lett. 86 (2001) 5970.
[15] R. Pincak and V.A. Osipov, Phys. Lett. A 314 (2003) 315.

[16] A. Krishnan, E. Dujardin, M.M.J. Treacy, J. Hugdahl, S. Lynum and T.W. Ebbesen, Nature 388 (1997) 451.
[17] Y.A. Kim, T. Hayashi, K. Osawa, M. Endo and M.S. Dresselhaus, Chem. Phys. Lett. 367 (2003) 537.
[18] S.P. Jordan and B.H. Crespi, Phys. Rev. Lett. 93 (2004) 255504.
[19] M. Ge and K. Sattler, Chem. Phys. Lett. 220 (1994) 192.
[20] M.S. Dresselhaus, G. Dresselhaus and P.C. Eklund, *Science of Fullerenes and Carbon Nanotubes* (Academic Press, California, 1995).
[21] H. Anton, *Calculus with Analytic Geometry* (Wiley Inc., Ny, USA, 1992).
[22] F.D. Colavecchia, G. Gasaneo and J.E. Miraglia, Comput. Phys. Comm. 138 (2001) 29.
[23] A. Erdélyi, *Higher Transcendental Functions* (McGraw-Hill, New York, 1953).
[24] I.S. Gradshteyn and I.M. Ryzhik, *Table of Integrals, Series, and Products* (Academic Press, San Diego, 2000).